Research Article | Vol. 30, No. 16 / 1 Aug 2022 / Optics Express 28632
Optics EXPRESS

Tunable narrow band add-drop filter design based on apodized long period waveguide grating assisted co-directional coupler

NABARUN SAHA, GIUSEPPE BRUNETTI, MARIO NICOLA ARMENISE, AND CATERINA CIMINELLI*

Optoelectronics Laboratory, Politecnico di Bari, Via E. Orabona 6, 70125 Bari, Italy
**caterina.ciminelli@poliba.it*

Abstract: Tunable add/drop filter based optical interconnects are an integral part of data centers as well as optical communications. Although add/drop filters based on ring resonators and waveguide Bragg gratings are well developed, long period waveguide grating (LPWG) based add/drop filters have little been investigated so far. In this article, we propose an apodized LPWG assisted co-directional coupler for narrow band add/drop filtering by combining silicon (Si) waveguide with titanium dioxide (TiO_2) waveguide geometry. The proposed structure has been analyzed by combining the finite element method (FEM) and transfer matrix method (TMM), showing a good side lobe suppression ratio (SLSR) equal to 25.7 dB and an insertion loss of 0.6 dB. Owing to the high group index difference of Si and TiO_2 waveguides, a narrow band response of 1.4 nm has been achieved with 800μm long LPWG. The opposite thermo-optic coefficients of Si and TiO_2 ensures a good thermal tunability of the central wavelength. Considering a thin metallic heater of titanium nitride (TiN) the thermal tuning efficiency is found to be 0.07 nm/mW. Further, two LPWGs have been cascaded to realize a tunable dual channel filter with a minimum channel spacing of 185 GHz and a channel crosstalk better than 20 dB, showing its potential application towards dense wavelength division multiplexing.

1. Introduction

Silicon based integrated optical waveguide devices have found numerous applications in the field of optical communications, data centers as well as microwave photonics due to their compatibility with complementary metal-oxide-semiconductor (CMOS) fabrication techniques as well as large integration density enabled by high index contrast. Further, the silicon photonic based devices also benefited from the high positive thermo-optic coefficient (TOC) of silicon which helps to realize efficient thermal tuning of the on-chip devices [1]. Over the years various silicon photonic devices have been proposed owing to these beneficial features. Here we focus on a narrow band add/drop filter, which is the most important element for various integrated photonic applications such as wavelength division (de) multiplexing (WDM).In order to cope with the growing demand of high efficiency optical interconnects, several add/drop filters based on arrayed waveguide gratings (AWGs) [2,3], Mach-Zehnder interferometers (MZIs) [4,5], ring resonators [6,7], waveguide Bragg gratings (WBGs) [8–10] have been reported in past two decades. Ring resonators based add/drop filters are one of the most preferred structures due to their compact footprint, sharp filtering response as well as structural simplicity and scalability. However, their performance is often limited by the free spectral range (FSR). Although the FSR can be increased significantly by cascading resonators having different ring radii [11], it makes the structure complicated.

Another popular photonic structure to realize add/drop filter is WBG, which is free from FSR, as required in many applications [12]. Since in WBGs the reflected mode propagates towards the input end, a circulator is required to separate the drop port from the input port. In recent time,

#461876 https://doi.org/10.1364/OE.461876
Journal © 2022 Received 25 Apr 2022; revised 7 Jun 2022; accepted 25 Jun 2022; published 20 Jul 2022

Optics EXPRESS

various CMOS compatible magneto-optic material based circulators have been reported [13–15] which can be used to separate the reflected mode at the input end. Although it seems promising and can add new dimension to the silicon photonics, the presence of circulators in WBG geometry also makes an as otherwise straightforward structure a bit complicated. Therefore, in order to separate the drop port from the input port, WBG has been realized in four port structure (input, through, add and drop) such as grating assisted contra-directional coupler [16,17] in which two highly asymmetrical waveguides are placed in parallel with sidewall gratings and the reflected spectrum can be received from the drop port. Another major issue with WBG add/drop filter is the presence of the strong side lobes which increases the cross talks between two adjacent channels. In order to reduce the side lobes, the gratings are often apodized, which can be implemented by modifying the corrugation amplitude or by introducing a relative phase between two sidewall gratings. For example, in Ref. [10] authors have reported an add/drop filter based on contra-directional coupler with phase apodization having 3-dB bandwidth and SLSR equal to 1 nm and 18 dB respectively. In another approach, a 3-dB bandwidth of 0.9 nm and a SLSR equal to 19 dB have been reported with single stage filtering [17]. The 3-dB bandwidth has been reduced further at the expense of an increase in insertion loss by dual stage filtering. Despite these promising performances such structures often suffer from errors due to the phase mismatch of two sidewall gratings originating from fabrication imperfections. The four port operation can also be realized by implementing WBG at the two arms of MZI [18,19]. For example, in Ref. [18] authors have reported an add/drop filter with a 3-dB bandwidth of 4 nm and a SLSR higher than 15 dB [18]. Although this approach is quite promising, mismatch in reflectivity associated with the gratings as well as phase mismatch between two arms can create distortion in the transmission spectrum. Alternatively, another promising development towards on-chip add/drop filterwith WBGs is using sidewall corrugated multimode waveguide combined with an adiabatic coupler [20–23]. Incorporating WBGs in multimode waveguides, a 3-dB bandwidth of 2.8 nm with SLSR equal to 20.5 dB have been reported in Ref [20]. WBGs in multimode waveguide provide best fabrication tolerances due to the large waveguide geometry but create issues like cross-coupling between many modes and requirement of adiabatic coupler which makes the structure complicated. Another major setback for WBGs is the small size of the grating teeth (~150 nm), making it difficult to realize an ideal rectangular shape. In addition, in almost all aforementioned geometries, a careful device design should be implemented to separate the resonance wavelength associated with inter-mode coupling from the intra-mode coupling.

Co-directional coupler based on long period waveguide grating (LPWG) can be a promising alternative as the period of the grating is of the order of micrometer and only intermodal coupling occurs [24,25]. The main hindrance in realizing narrow band on-chip add/drop filters based on LPWG is the inherent small group index difference (~0.1) of theparticipating modes in silicon geometry to which the bandwidth is inversely proportional. Therefore, in order to realize a narrow bandwidth spectrum, a centimeter order of grating length is usually required which not only is against device compactness but also makes it vulnerable to fabrication imperfections. It is to note that unlike WBGs, in LPWG-assisted devices the thermal tuning of the central wavelength depends on the differential thermal dependence of two participating modes. As a result, both the modes show unidirectional thermal dependence in a Si-Si parallel combination structure, making it difficult to establish a good thermal tuning efficiency as well. To the best of our knowledge, the only add/drop filter based on LPWG has been reported in Ref. [26] where an innovative design including two sidewall corrugated silicon waveguides with a vertically loaded silicon-nitride waveguide structure provided a narrow bandwidth of 1.16 nm with an 1.1 mm long LPWG. In this paper, we have combined the silicon waveguide with another CMOS compatible material as titanium dioxide (TiO_2) for the second waveguide in simple parallel configuration to achieve a narrow band add/drop filter as well as good thermal tunability of the central wavelength. Recently, the TiO_2 based waveguide devices have gained much attention due to their high index

Optics EXPRESS

contrast, low loss in the telecommunication window as well as a high negative thermo-optic coefficient (TOC) [27,28]. Due to the negative TOC of the TiO_2, in various configurations it has been used with a Si waveguide to realize athermal operation [29,30]. In the proposed structure, the TiO_2 waveguide has been placed in parallel with a Si waveguide to enhance the thermal tuning efficiency using the opposite TOC of the two materials. In addition, the small wavelength dependence of the TiO_2 waveguide as compared to the Si waveguide has been utilized to reduce the bandwidth to 1.4 nm with a small grating length of 800 μm. The apodized grating has been placed in between the wide space of two waveguides which establishes an SLSR equal to 25.7 dB. The thermaltunning efficiency of the proposed structure has also been characterized with a thin metallic heater which is found to be 0.07 nm/mW. Further, it has been shown that by cascading two LPWGs a dual channel drop filter can be generated with minimum channel spacing of 185 GHz by varying the electric power in metallic heater placed over each grating. The calculations have been performed using 3D finite element method (FEM) and transfer matrix method (TMM).

2. Device design and theoretical modeling

The 3D schematic of the proposed filter structure as well as the cross-sectional view is illustrated in Fig. 1. It consists of a silicon (Si) strip and a titanium dioxide (TiO_2) waveguide placed parallel to each other with a wide space in between. The width of the Si strip (W_s)and TiO_2 strip (W_t) is considered to be 320 nm and 900 nm, respectively, whereas the thickness of both the waveguides (H) is considered to be 280 nm. The chosen dimensions ensure single mode operation for both the waveguides in the operating range of telecommunication wavelength (C + L band). The entire structure is covered with a silica (SiO_2) upper cladding. The gap between the two waveguides (G) is considered to be 1 μm in order to suppress any cross-coupling in the absence of the grating.

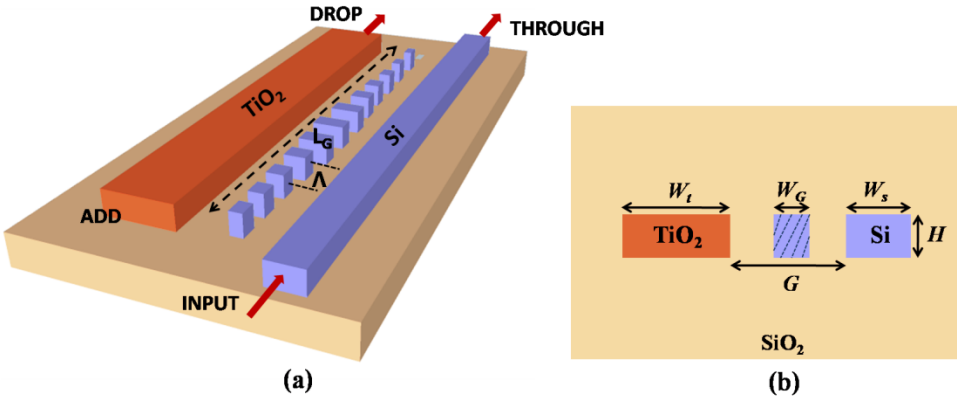

Fig. 1. (a) 3D Schematic diagram and (b) cross-sectional view of the proposed filter.

In Fig. 2 we have plotted the variation of crossed fractional modal power (FMP) associated with the quasi-TE mode of Si waveguide (TiO_2 waveguide) to TiO_2 waveguide (Si waveguide) represented by red (blue) curve. The crossed FMP starts to saturate around 800 nm and becomes nearly 0 around 1 μm. The long period grating is considered to be formed by a periodic array of Si rectangles with 50% duty cycle placed at the middle of two waveguides with a grating pitch of 4.2 μm such that the resonance occurs around 1.55 μm.

Optics EXPRESS

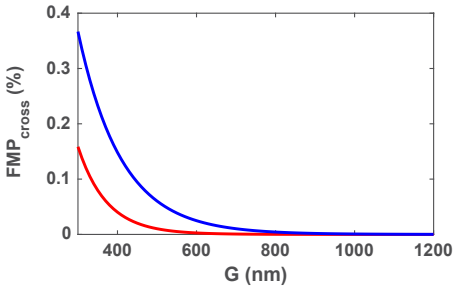

Fig. 2. Variation of crossed fractional modal power (FMP) at two waveguides as a function of gap (G) between two waveguides.

The widths of the Si rectangles are designed as a Gaussian function along the direction of propagation, governed by the equation,

$$W_G = W_{\max} \exp\left(-\eta \frac{(z - 0.5L_G)^2}{L_G^2}\right) \tag{1}$$

where, $W_{\max}$ is the maximum grating width placed at z = $L_G/2$, and η is the apodization strength. In the proposed structure the fundamental TE mode excited in the Si waveguide couples to the TiO_2 waveguide through evanescent field coupling by the intermediate grating. The coupling is maximum at the phase matching condition given by $\lambda_R = \Delta n_e \Lambda$ where $\Delta n_e = (n_{esi} - n_{tio_2})$ is the modal effective index difference between the participating modes and Λ is the grating period. The transmission spectrum of the proposed structure has been calculated using the TMM in which the grating has been divided into m number of sections with equal length L_m in which the output amplitude at the through and drop port is related to the input via the sequential multiplication of adjacent transfer matrices given as [31,32],

$$\begin{pmatrix} A(L_G) \\ B(L_G) \end{pmatrix} = T \begin{pmatrix} A(0) \\ B(0) \end{pmatrix} \text{ where, } T = \prod_m T_m \tag{2}$$

where, T_m is the 2×2 transfer matrix of the m^{th} section consisting of four elements given by,

$$\left.\begin{aligned} T_{11}^m &= \exp(i(\beta_1 - \sigma)L_m)\left[\cos(\gamma_m L_m) + \tfrac{i\sigma}{\gamma_m}\sin(\gamma_m L_m)\right] \\ T_{12}^m &= \tfrac{i\kappa_m}{\gamma_m}\exp(i(\beta_1 - \sigma)L_m)\exp(2\pi i^{z_m}/_{\Lambda})\sin(\gamma_m L_m) \\ T_{21}^m &= \tfrac{i\kappa_m}{\gamma_m}\exp(i(\beta_2 + \sigma)L_m)\exp(-2\pi i^{z_m}/_{\Lambda})\sin(\gamma_m L_m) \\ T_{22}^m &= \exp(i(\beta_2 + \sigma)L_m)\left[\cos(\gamma_m L_m) - \tfrac{i\sigma}{\gamma_m}\sin(\gamma_m L_m)\right] \end{aligned}\right\} \tag{3}$$

In the above equations, $\beta_1 = 2\pi n_{esi}/\lambda + i\alpha_1$ and $\beta_2 = 2\pi n_{etio_2}/\lambda + i\alpha_2$ are the complex propagation constants of the Si and TiO_2 waveguides respectively with α_1 and α_2 being the field attenuation coefficients, $z_m = (m-1)L_m$ is the initial position of the m^{th} section, $\sigma = (\beta_1 - \beta_2)/2 - \pi/\Lambda$ is the detuning parameter and $\gamma_m\sqrt{(\sigma^2 + |\kappa_m|^2)}$, where κ_m is the coupling coefficient of the m^{th} section given by [33],

$$\kappa_m = \frac{n_{si}^2 - n_{sio_2}^2}{2\lambda c\mu_o} \iint_{A_m} \boldsymbol{E}_{si} \cdot \boldsymbol{E}_{tio_2} dA \tag{4}$$

where, $\boldsymbol{E}_{si}$ and $\boldsymbol{E}_{tio_2}$ are the power normalized electric field components of the Si and TiO_2 waveguides respectively. The field components and the modal effective indices have been obtained

Optics EXPRESS

using full vectorial FEM. The integration has been carried out in the grating area (A_m) for the m^{th} section in which the grating has been replaced by a uniform waveguide with average refractive index between perturbed and unperturbed waveguide, i.e. $(n_{si} + n_{sio_2})/2$ [33]. The grating length is considered to be one coupling length that obeys the condition $\sum \kappa_m L_m = \pi/2$[29]. Considering that only the Si-mode excited at the input end, the output spectrum at the through port and drop port can be obtained following the expression $P_{through} = |A(L_G)|^2$ and $P_{drop} = |B(L_G)|^2$, respectively. The 3-dB bandwidth of the spectrum is estimated to be [33,34],

$$\Delta\lambda_{3dB} = 0.8\frac{\lambda_R^2}{L_G \Delta N_g} \tag{5}$$

In the above expression, ΔN_g is the group index difference between the participating modes given by, $\Delta N_g = \Delta n_e - \lambda\partial(\Delta n_e)/\partial\lambda$. The temperature sensitivity of the proposed structure is governed by [35],

$$\frac{d\lambda_R}{dT} = \frac{\lambda_R}{\Delta N_g}\frac{\partial(\Delta n_e)}{\partial T} \tag{6}$$

In order to account the wavelength dependence, the refractive indices of SiO_2, Si and TiO_2 have been obtained using corresponding Sellmeier relations [36–38],whereas, the temperature dependence has been accounted through the linear relation $n_T = n_{T_0} + dn/dT(T - T_o)$[36] where n_{T_0} is the refractive index at the room temperature. In the above equation dn/dT is the thermo-optic coefficient which is taken as 1.06×10^{-5}, 1.8×10^{-4}, -2×10^{-4}/°C for SiO_2, Si and TiO_2, respectively [39,40,30].

3. Results and discussions

In the conventional Si-Si structure the major reason for LPWGs being not so popular for add-drop multiplexing is the difficulty in realizing narrow bandwidth spectrum with shorter grating length. In order to overcome this issue, in the reported structure we have combined a TiO_2 waveguide with the Si waveguide geometry. As it appears from Eq.5, the bandwidth of the LPG is inversely proportional to the group index difference ΔN_g, which largely relies on the wavelength dependence of the participating modes. In order to highlight the benefits of the proposed configuration, in Fig. 3(a)ΔN_g has been plotted as a function of wavelength for the proposed TiO_2-Si waveguide (blue curve) and a conventional Si-Si waveguide (red curve). Here we like to mention that TiO_2-Si waveguide refers to the proposed structure, i.e. the parallel combination of a TiO_2 and a Si waveguide whereas Si-Si structure implies a parallel combination of two Si waveguides which has been studied widely for add-drop filtering applications. In order to compare the proposed structure with state-of-the-art Si-Si waveguide, we have considered commonly used waveguide dimension for add-drop filter which is 600 nm and 400 nm in width, 220 nm in height and a separation of 300 nm to ensure single mode operation as well as avoid any coupling in the absence of grating as reported in [10,17]. The features of the proposed TiO_2-Si structure are mentioned in the previous section. As can be seen from the Fig. 3(a), for the proposed structure ΔN_g is almost one order higher as compared to the Si-Si structure for co-directional coupling. This can be attributed to relatively weak wavelength dependency of the TiO_2 waveguide as compared to the Si waveguide. As a result, the group index of the TiO_2 waveguide is found to be lower than the Si-waveguide. For example, at $\lambda = 1.55$ µm, the group index of the TiO_2 and Si waveguides is found to be 2.36 and 4.57 respectively, resulting a large $\Delta N_g = 2.21$. On the other hand, for the Si-Si structure, the wavelength dependency of the participating modes is almost identical. At $\lambda = 1.55$ µm, the group index of the two Si waveguides is found to be 4.36 and 4.04 respectively, resulting a small index difference $\Delta N_g = 0.32$.

Here it is to note that the temperature sensitivity or thetuning of the resonance wavelength is inversely proportional to ΔN_g[see Eq.6]. Thus, the increment in ΔN_g, reduces the temperature

Optics EXPRESS

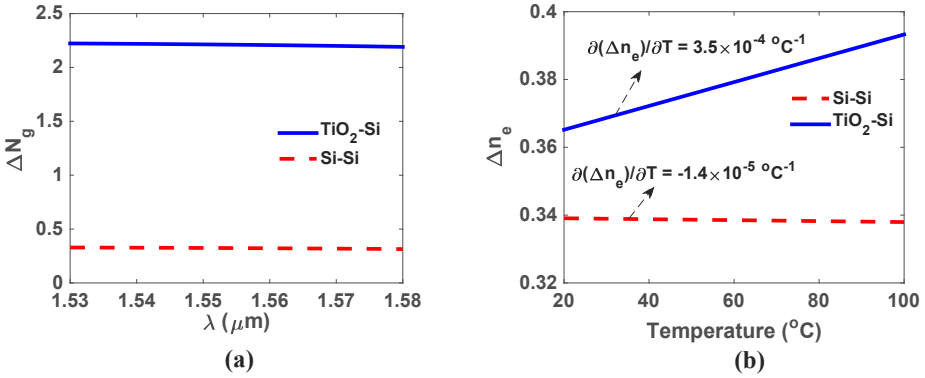

Fig. 3. (a) Variation of ΔN_g with wavelength and (b) Δn_e with temperature for the proposed TiO_2-Si structure and a conventional Si-Si structure.

sensitivity, making it imperative to increase the participating mode's thermal dependence to achieve a good tuning efficiency. In this context, the proposed structure is benefited from large negative TOC of the TiO_2 as well as large positive TOC of Si waveguide. Due to the large opposite TOC characteristics of TiO_2 and Si, the thermal dependence on the factor Δn_e increases significantly. In order to quantitatively find out the enhancement, the variation of Δn_e with temperature for the proposed structure as well as for a conventional Si-Si structure is shown in Fig. 3(b), where the Δn_e increases linearly with temperature with a much better slope efficiency ($\partial(\Delta n_e)/\partial T$) as compared to the Si-Si waveguide. The value of $\partial(\Delta n_e)/\partial T$ is found to be 3.5×10^{-4}/°C for the proposed structure whereas it is only -1.4×10^{-5}/°C for Si-Si waveguide, showing a 25 times enhancement in $\partial(\Delta n_e)/\partial T$ leading to an increment in sensitivity [see Eq.6]. The temperature sensitivity is found to be 246 pm/°C for the TiO_2-Si structure which is 3.7 times higher than the Si-Si structure in co-propagation configuration (67 pm/°C). The sensitivity is also found to be higher as compared to conventional counter-propagating Si-Si structure with WBG (76 pm/°C). Above, to compare the proposed structure with the state-of-the-art Si-Si structure, the thickness of the two structures is considered to be different, 220 nm and 280 nm for Si-Si and TiO_2-Si respectively. In order to compare the proposed structure performance with respect to a 280 nm thick Si-Si structure, the factor ΔN_g and $\partial(\Delta n_e)/\partial T$ also has been calculated for the same, which is found to be 0.28 and 1.08×10^{-5} /°C respectively. Therefore, the enhancement in the factor ΔN_g ($\partial(\Delta n_e)/\partial T$) is found to be 7.8 (32) and 6.9 (25) with respect to 280 nm thick and 220 nm thick Si-Si structure, demonstrating a remarkable improvement of the performance of the proposed geometry.

In order to obtain the transmission spectrum with high SLSR,the target apodization profile is mapped in the grating width placed at the middle of two waveguides following Eq.1. The corresponding coupling coefficient (κ μm^{-1}) has been calculated by using Eq.4 which is plotted in Fig. 4 as a function of grating width.It shows a nonlinear behavior with the grating width which has been fitted with a third order polynomial that can be expressed as,

$$\kappa = 3.51\times10^{-10}W_G^3 - 1.6\times10^{-7}W_G^2 + 3.1\times10^{-5}W_G - 0.0018 \quad (7)$$

The variation of W_G and the corresponding coupling coefficient as a function of grating length for three different grating strengths,1, 2 and 4, keeping the maximum width (W_{max}) fixed at 320 nm are shown in Fig. 5(a) and (b), respectively. If the apodization strength is small (η= 1), the coupling coefficient variationis found to be very weak.

On the other hand, for stronger strength ($\eta = 4$), the apodization is sharper in the central part of the grating due to the non-linear characteristics of the coupling coefficient with the grating width.

Optics EXPRESS

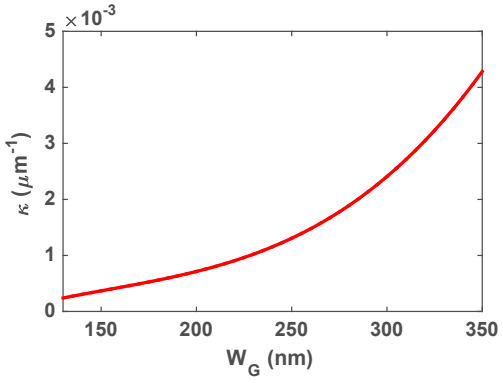

Fig. 4. Variation of coupling coefficient with grating width for the proposed structure

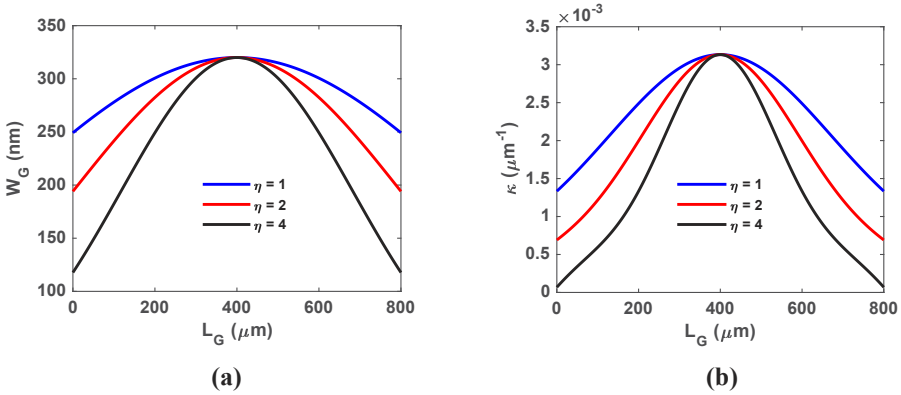

Fig. 5. (a) Variation of grating width W_G and (b) coupling coefficient with grating length L_G for three different apodization strength.

In both cases it is difficult to achieve a good SLSR. Therefore, in the following calculation an intermediate apodization strength $\eta = 2$ has been considered. This approach leads to a minimum grating width required for this apodization to be 194 nm, which can be accomplished conveniently using CMOS compatible lithographic techniques.

Considering the aforementioned grating and waveguide parameters the transmission spectrum has been calculated with a grating length of 800 μm. The propagation losses are considered to be 5 dB/cm and 10 dB/cm for the TiO_2 and Si waveguide, respectively [27,41]. Although it is possible to achieve almost one order less propagation loss with the current fabrication technologies [28,42–44], the losses are considered to be higher to account for all sort of fabrication imperfections as well as material absorption. The through and drop port spectrum of the proposed apodized grating filter in shown in Fig. 6. In order to show a comparison, in the inset the through port spectrum for a uniform grating is also reported. The SLSR is found to be 25.7 dB for the apodized grating which is much better as compared to 9.7 dB achieved with the uniform grating. The 3-dB bandwidth is found to be 1.4 nm (179 GHz), lowest reported bandwidth so far with micrometer order grating length based on LPWGs, to the best of our knowledge. The insertion loss at the drop channel port is found to be only 0.6 dB. In order to study the fabrication tolerances, we have plotted the variation of SLSR and insertion loss (IL) as a function of maximum grating width (W_{max}) and grating strength (η) in Fig. 7(a) and 7(b), respectively. In both figures the variation in W_{max} is considered to be from 300 to 340 nm whereas it is from 1.8 to 2.2 in grating

Optics EXPRESS

strength. It is to note that variation of ± 0.2 in grating strength for a fixed W_{max} results in ±10 nm variation in the minimum grating. An accuracy of this order can be accomplished easily with the CMOS compatible fabrication techniques [45]. As it can be visible from the Fig. 7(a) even with simultaneous inaccuracy of ± 20 nm in W_{max} and ± 0.2 in η it is possible to achieve SLSR higher than 20 dB, showing a good tolerance in terms of apodization parameters. The insertion loss (Fig. 7(b)) is found to be stable in terms of grating strength whereas showing a relatively sharp variation with W_{max} caused by a strong dependence of coupling strength and thus of the coupling length on W_{max}. Since the grating length is considered to be one coupling length corresponding to the apodized grating with W_{max} = 320 nm, a deviation in W_{max} leads to deviation of the coupling length from the considered grating length.

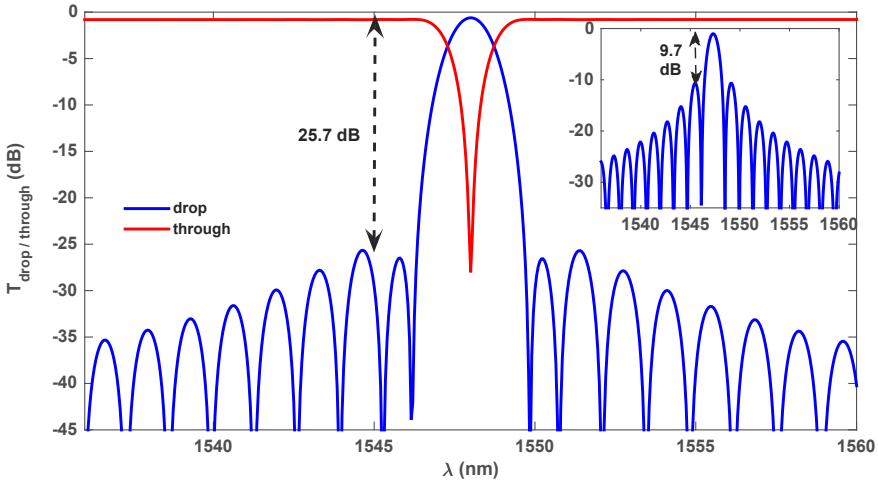

Fig. 6. Drop port and through port spectrum of the proposed structure. Inset is showing the drop port spectrum of the uniform grating structure.

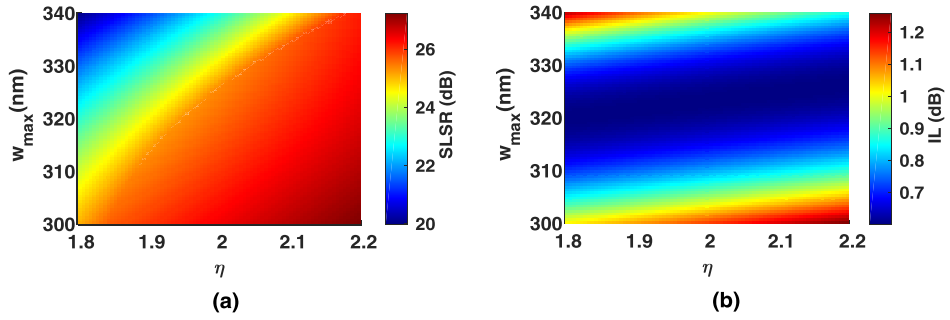

Fig. 7. Surface plot of (a) side lobe suppression ration (SLSR) and (b) insertion loss (IL) as a function of maximum grating width (W_{max}) and grating strength (η).

Owing to the fact that for LPWG, the peak transmittance shows a periodic variation with grating length having maximum transmittance at one coupling length, the deviation of coupling length from the selected grating length results in under coupling or over coupling. This leads to an increment in insertion loss. Despite this behavior, the insertion loss is still found to be ∼1 dB.

In order to actively tune the position of the resonance wavelength a 60 nm thin layer of Titanium Nitride (TiN) micro-heater is widely placed over the waveguide structure. The TiN has been

Optics EXPRESS

considered as a metallic heater since it shows a good resistance against corrosion and have good chemical and thermal stability [4,40]. The thickness of the TiN heater is considered to be 60 nm, as it is relatively easy to form a thin metallic layer. The width of the TiN heater is considered to be 2.5 μm so that it covers the entire structure whereas the separation between the TiN heater and the waveguide is taken as 1 μm to minimize any additional propagation loss originating due to the metallic absorption. The electro thermo-optic simulations have been carried out by using a 3D FEM approach. The simulations have been performed considering a buried oxide layer of thickness equal to 2 μm in between a thick silicon substrate of 20 μm and the waveguide structure. The left and right boundaries are also considered to be 20 μm apart from the central part of the waveguide structure. The left, right and bottom boundaries are considered to be at room temperature ($T_o = 20°C$) whereas a convective boundary condition has been used for the top layer. The current flow through the TiN layer generates heat flow in the structure which induces a temperature distribution in the structure as shown in Fig. 8. The change in the applied electric power in TiN heater results in a change in the temperature of the waveguide cores which induces shifts in the resonance wavelength.The drop port spectrum for three different applied electric powers is shown in Fig. 9(a), which shows a red shift with the increment in applied power.

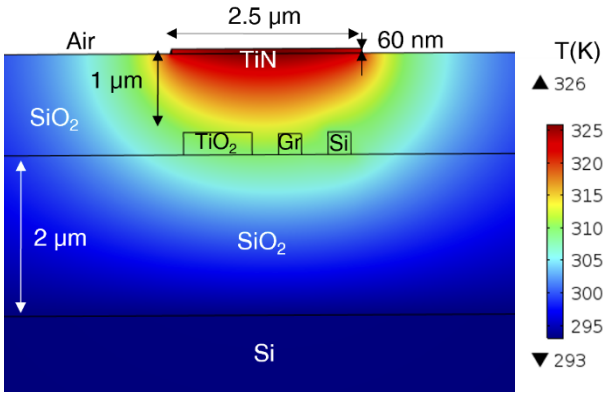

Fig. 8. Temperature distribution due to current flow in the TiN heater. Gr: grating.

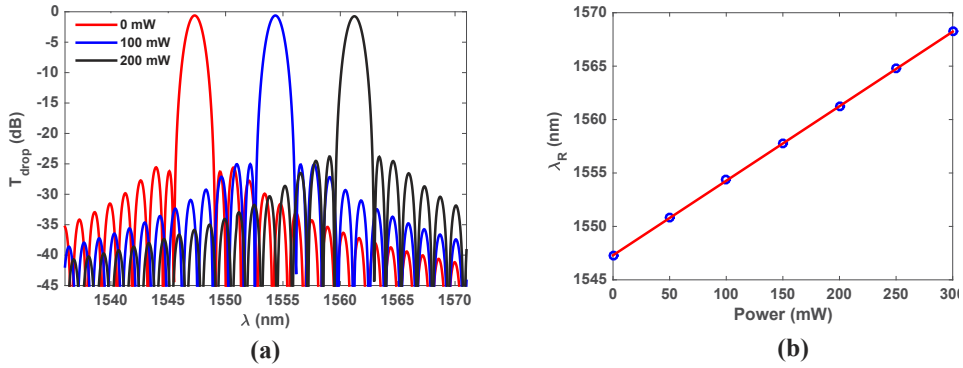

Fig. 9. (a) Drop port spectrum for three different electric powers.(b) Shift of the resonance wavelength with the electric powers.

The shift of theresonance wavelength with the increase in applied power shows a linear characteristic with the tuning efficiency 0.07 nm/mW (see Fig. 9(b)). The tuning efficiency can

Optics EXPRESS

be enhanced further by creating air trenches as reported in literature [46,47]. The normalized thermal response of the proposed structure is shown in Fig. 10 with a voltage pulse. The 10-90% rising time is found to be 9.94 µsec whereas 90-10% falling time is 9.75µsec.

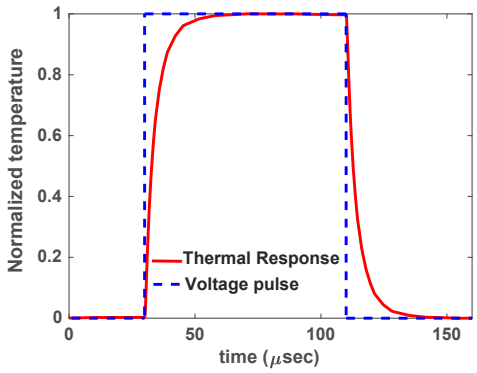

Fig. 10. Thermal response of the proposed structure with a voltage pulse.

A comparison of the proposed structure with results reported in literature for WBG structures and one with LPWG structure [26] is shown in Table 1. The proposed structure shows good performance compared to the different innovative structures reported for channel drop filtering applications. In particular the insertion loss is lowest among all the filters despite considering one order higher loss as compared to recently reported losses in Si and TiO_2 waveguide [28,42–44]. The insertion loss can be further reduced to ~ 0.1 dB considering the recently reported propagation losses in Si waveguide (1-2 dB/cm) [42–44] and TiO_2 waveguide (0.6-1 dB/cm) [28,48]. The reason behind the lower insertion losses compared to all the WBG structures can be attributed to the LPWG's unique band pass characteristic. In LPWGs it is possible to achieve a perfect band pass filtering with zero insertion loss at grating length equal to coupling length considering loss less medium. On the other hand, the peak reflectivity of WBGs shows an asymptotic behavior with length making it impossible to realize perfect band pass characteristics with zero insertion loss with finite length even in loss less medium.

Table 1. Comparison of the device performance with earlier reported structures.

Ref.	Bandwidth (nm)	SLSR (dB)	Tuning efficiency (nm/mW)	Insertion loss (dB)	Grating Length (µm)
[10]	1	18.6	0.017	1.6	495
[16]	-	30	-	1.2	829
[20]	9.5	22	-	0.8	200
[17]	0.9	19	0.006	1.3	900
[22]	40	24	0.16	1	100
[21]	16.5	21	-	1	600
[19]	3.5	40	-	5	960
[18]	4	15	-	-	1500
[23]	2.8	20.5	0.029	1.2	472
[25]	1.16	5	-	-	1130
Proposed structure	1.4	25.7	0.07	0.6	800

Optics EXPRESS

The proposed structure can be cascaded to realize a multi-channel optical filter. As an example, we have cascaded two LPWGs to form dual channel optical filter in which the through port of the first waveguide has been cascaded with the input of the second waveguide. The grating period is considered to be the same for both LPWG structures. The metallic heater placed over each LPWG enables tuning of each channel individually as well as controlling the channel spacing. The separation between the cascaded LPWG structures (L_{sep}) is considered to be 100 μm to avoid any possibility of cross heating of the two LPWG structures due to the power variation in individual heater. In Fig. 11 we have plotted the dual channel spectrum for two different heating powers equal to 10 mW and 20 mW applied at the second TiN heater, keeping the power in the first heater at 0 mW. Figure 11 clearly shows that power change in the second heater does not affect the spectrum of the first channel (Ch1) whereas second channel (Ch2) shows a red shift. Since the increase of the heating power leads to resonance wavelength shift only for the second LPWG, for a certain power value, the resonance wavelength of the second LPWG will move away from the throughput stop band of the first LPWG, with an improvement of the insertion loss.

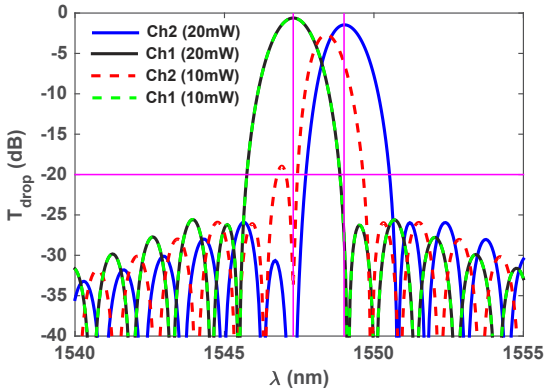

Fig. 11. The drop port spectrum of dual-channel cascaded LPWG structure for two different heating powers at the second TiN heater.

This effect is clearly shown in Fig. 11, by comparing the dotted red and blue lines, referred to the drop port of Ch2 for power of 10 mW and 20 mW, respectively. In particular, for power equal to 10 mW, the resonance wavelength of the second LPWG is still within the stop band of the first LPWG's through port, resulting in high insertion loss. For power equal to 20 mW, the resonance wavelength of the second LPWG moved away from the stop band, resulting in a reduction of insertion loss of the drop port. Therefore, the minimum channel spacing is set as the distance between the resonance wavelengths of two channels when the insertion loss of both channels is minimum as highlighted by two vertical lines. In this case, the minimum channel spacing is 1.47 nm (185 GHz) (see Fig. 11). The mismatch of the insertion loss in both channels (insertion loss of Ch2 is around 1.6 dB higher of the Ch1), since Ch2 light covers both the LPWGs as well as the spacing between two waveguides. The crosstalk between the two channels is defined as the difference, expressed in dB, between the transmittance of Ch2 (Ch1) with respect to Ch1 (Ch2) at the peak of each channel [21,49]. As highlighted by the purple lines in Fig. 11, the crosstalk for both channels is larger than 20 dB for bandwidth of 1.7 nm and 1.4 nm for Ch1 and Ch2, starting from 1546 and 1548.9, respectively. Since in dense wavelength division multiplexing system a channel spacing around 200 GHz is needed, the proposed structure can be a promising development towards it.

It is important to note that, random variations in structural parameters along the length originating due to fabrication imperfection can cause a significant effect on filter response, especially the SLSR [20,21]. Therefore, considering a random local error of ±10 nm along the

Optics EXPRESS

length from the nominal values in each device parameters (as expected by the state-of-the-art manufacturing approaches [45,50]), a statistical analysis has been performed to study its effect on SLSR. It has been observed that such a variation causes two effects, local phase change $\phi(z)$ due to the local modal effective index variation and local change in the modal overlap in the grating section and thus the coupling coefficient $\kappa(z)$. Therefore, considering a large number of errors (between 10 to 100) in each grating sections and N number of different combinations of such errors over the entire device length, the effect of random variations in structural parameters on SLSR has been investigated based on $\phi(z)$ and $\kappa(z)$. In order to reduce the computational time and volume, first the investigation is carried out separately for $\phi(z)$ and $\kappa(z)$, based on which the most critical parameter has been identified and finally the combined effect of $\phi(z)$ and $\kappa(z)$ has been studied for the critical parameter. For example, in Fig. 12(a) and (b) the distribution of SLSR has been shown separately for $\phi(z)$ and $\kappa(z)$ occurring due to ±10 nm errors in W_s and W_t and ±5 nm errors in W_s. Figure 12 (a) shows that the spread in SLSR is much higher for Si waveguide as compared to the TiO_2 waveguide. The corresponding mean value and standard deviation (Std) is found to be 22.01 dB and 1.6 dB for ±10 nm errors in W_s whereas 25.5 dB and 0.09 dB for ±10 nm errors in W_t. The larger deviation in SLSR for Si waveguide can be attributed to the combined effect of the higher index contrast of the Si waveguide and the discontinuity of electric field component in the direction of width for the TE mode, leading to larger variation in local modal effective index and thus $\phi(z)$ for the Si waveguide. This shows that the device demand better accuracy in terms of W_s. In view of this, in the figure the distribution of SLSR is also plotted by considering ±5 nm variation in W_s which shows a significant improvement. The corresponding mean and Std is found to be 23.96 dB and 0.92 dB. In Fig. 12 (b) the SLSR distribution is plotted to study the effect of $\kappa(z)$ due to the errors in width.

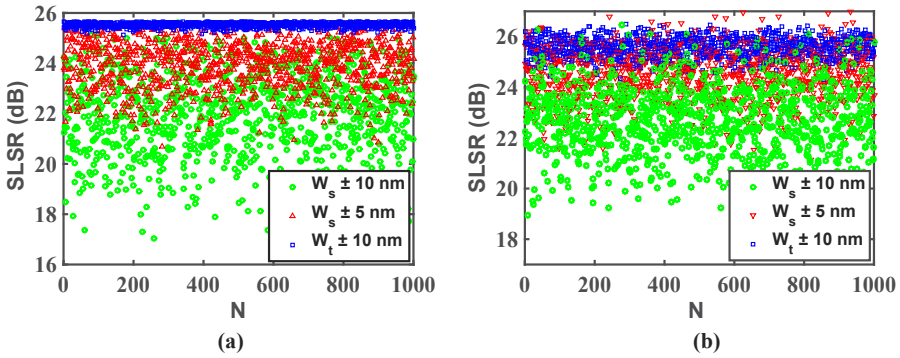

Fig. 12. Statistical distribution of SLSR corresponding to (a) $\phi(z)$ and (b) $\kappa(z)$ for N number of different combinations of errors in Si and TiO_2 waveguide's width along the length.

Again, the SLSR is found to be more vulnerable to W_s due to the higher index contrast of Si waveguide, for which the mode confinement affected strongly with slight variations in width. As a result, the modal overlap in the grating section becomes more susceptible to W_s as compared to W_t. The mean SLSR and corresponding Std is found to be 22.68 dB and 1.36 dB for ±10 nm variations in W_s and 25.57 dB and 0.4 dB for ±10 nm variations in W_t. The device shows a better performance for ±5 nm errors in W_s with mean SLSR 24.5 dB and Std 0.96 dB. The mean value of SLSR and Std is found to be 23.98 dB (24.95 dB) and 0.93 dB (0.46 dB) for ±10 nm errors in the thickness in Si (TiO_2) corresponding to $\phi(z)$ whereas 24.78 dB (24.9 dB) and 0.88 dB (0.79 dB) corresponding to $\kappa(z)$. The device behaves better with respect to height variations and also the difference between the mean values of SLSR for Si and TiO_2 waveguide is smaller as compared to width variation. These characteristics can be attributed to the absence of field discontinuity in the direction of height which causes smaller changes in local effective index for

Optics EXPRESS

the Si waveguide as compared to width variations. On the other hand the variations in height causes smaller change in the modal overlap in the grating section and thus the $\kappa(z)$ in the grating sections for Si waveguide. The effect of height for the TiO_2 waveguide on SLSR is found to be slightly higher as compared to width, as the field confinement in the direction of height is relatively weak. Owing to the fact that the modal field in the grating section is very small, the device shows a stable performance with respect to the variations in grating's width and height as well as length of each grating sections. For example, the mean SLSR is found to be 25.6 dB (24.23 dB) corresponding to $\phi(z)$ ($\kappa(z)$) for a ±10 nm variations in W_G whereas 25.62 dB (25.16 dB) for a ±10 nm variations in H_G. This analysis shows that the most critical parameter of the proposed structure is the width of the Si waveguide W_s. Therefore, considering ± 10 nm and ± 5 nm errors in W_s, a combined effect of $\phi(z)$ and $\kappa(z)$ on SLSR has been investigated. The mean and Std is found to be 20.4 dB and 1.7 dB for ± 10 nm whereas 23.1 dB and 1.06 dB for ± 5 nm. It concludes that, in order to have better device performance the variation in W_s should be within ± 5 nm which can be accomplished with e-beam lithography technique as reported in Ref. [51,52]. Following this analysis, below a step by step possible fabrication technique has been discussed based on the reported and well-known fabrication techniques [28,33,53]. In the first step of the fabrication, a channel can be created using e-beam lithography and reactive ion etching on a silicon-on-insulator wafer with 280 nm Si top for TiO_2 waveguide formation [43]. The TiO_2 layer can be deposited using RF magnetron sputtering with titanium (Ti) target in oxygen environment [28]. The second step of e-beam lithography and reactive ion etching can be used to selectively form the Si-waveguide and the intermediate grating with desired variations in width along the grating length [33,54]. Besides, the SiO_2 cladding can be formed following plasma enhanced chemical vapor deposition [17]. Finally, the TiN micro-heater can be deposited using DC magnetron sputtering [55].

4. Conclusions

A thermally tunable add/drop filter based on long period grating has been demonstrated combining the beneficial features of silicon and TiO_2 waveguides. The long period grating has been placed in between the two waveguides with apodized grating width to realize high SLSR = 25.7 dB. A narrow bandwidth (1.4 nm) has been achieved with only 800μm long LPWG owing to the large group index difference between the guided modes of Si and TiO_2 waveguides. In addition, the large opposite TOC of Si and TiO_2 induces a 25 times enhancement in differential thermal dependence of the participating modes. As a result, a good thermal tuning efficiency 0.07 nm/mW has been achieved with a thin TiN metallic heater. The 10-90% rising (90-10% falling) time is found to be 9.94 μsec (9.75 μsec). Further, cascading two LPWGs a channel spacing of 185 GHz has been demonstrated between dual-channel with only 20 mW electric power in the second heater. The proposed structure is a promising development towards dense wavelength division multiplexing with LPWG assisted co-directional coupler.

Funding. Ministero dell'Istruzione, dell'Università e della Ricerca (NSG_ARS01_01215).

Disclosures. The authors declare no conflicts of interest.

Data availability. Data underlying the results presented in this paper are not publicly available at this time but may be obtained from the authors upon reasonable request.

References

1. G. Brunetti, N. Sasanelli, M. N. Armenise, and C. Ciminelli, "High performance and tunable optical pump-rejection filter for quantum photonic systems," Opt. Laser Technol. **139**, 106978 (2021).
2. S. Chen, X. Fu, J. Wang, Y. Shi, S. He, and D. Dai, "Compact Dense Wavelength-Division (De)multiplexer Utilizing a Bidirectional Arrayed-Waveguide Grating Integrated With a Mach–Zehnder Interferometer," J. Lightwave Technol. **33**(11), 2279–2285 (2015).
3. S. Tondini, C. Castellan, M. Mancinelli, C. Kopp, and L. Pavesi, "Methods for low crosstalk and wavelength tunability in arrayed-waveguide grating for on-silicon optical network," J. Lightwave Technol. **35**(23), 5134–5141 (2017).

Optics EXPRESS

4. G. Brunetti, G. Marocco, A. Di Benedetto, A. Giorgio, M. N. Armenise, and C. Ciminelli, "Design of a large bandwidth 2× 2 interferometric switching cell based on a sub-wavelength grating," J. Opt. **23**(8), 085801 (2021).
5. L. Zhou and A. W. Poon, "Fano resonance-based electrically reconfigurable add–drop filters in silicon microring resonator-coupled Mach–Zehnder interferometers," Opt. Lett. **32**(7), 781–783 (2007).
6. G. Brunetti, F. Dell'Olio, D. Conteduca, M. N. Armenise, and C. Ciminelli, "Ultra-compact tuneable notch filter using silicon photonic crystal ring resonator," J. Lightwave Technol. **37**(13), 2970–2980 (2019).
7. C. Ciminelli, F. Dell'Olio, G. Brunetti, D. Conteduca, and M. N. Armenise, "New microwave photonic filter based on a ring resonator including a photonic crystal structure," *19th International Conference on Transparent Optical Networks (ICTON) (pp. 1-4)*. IEEE, pp.1–4 (2017).
8. K. Abdelsalam, E. Ordouie, M. G. Vazimali, F. A. Juneghani, P. Kumar, G. S. Kanter, and S. Fathpour, "Tunable dual-channel ultra-narrowband Bragg grating filter on thin-film lithium niobate," Opt. Lett. **46**(11), 2730–2733 (2021).
9. Y. Ma, Y. Zhao, Y. Shi, L. Hao, Z. Sun, Z. Hong, and X. Chen, "Silicon Add-Drop Multiplexer Based on π Phase-Shifted Antisymmetric Bragg Grating," IEEE J. Quantum Electron. **57**(4), 1–8 (2021).
10. H. Qiu, J. Jiang, P. Yu, D. Mu, J. Yang, X. Jiang, H. Yu, R. Cheng, and L. Chrostowski, "Narrow-Band Add-Drop Filter Based on Phase-Modulated Grating-Assisted Contra-Directional Couplers," J. Lightwave Technol. **36**(17), 3760–3764 (2018).
11. W. Bogaerts, P. De Heyn, T. Van Vaerenbergh, K. De Vos, S. Kumar Selvaraja, T. Claes, P. Dumon, P. Bienstman, D. Van Thourhout, and R. Baets, "Silicon microring resonators," Laser Photonics Rev. **6**(1), 47–73 (2012).
12. W. Zhang and J. Yao, "A fully reconfigurable waveguide Bragg grating for programmable photonic signal processing," Nat. Commun. **9**(1), 1396 (2018).
13. P. Pintus, D. Huang, P. A. Morton, Y. Shoji, T. Mizumoto, and J. E. Bowers, "Broadband TE Optical Isolators and Circulators in Silicon Photonics Through Ce:YIG Bonding," J. Lightwave Technol. **37**(5), 1463–1473 (2019).
14. W. O. F. Carvalho and J. R. Mejía-Salazar, "Magneto-optical micro-ring resonators for dynamic tuning of add/drop channels in dense wavelength division multiplexing applications," Opt. Lett. **46**(10), 2396–2399 (2021).
15. T. Murai, Y. Shoji, N. Nishiyama, and T. Mizumoto, "Nonvolatile magneto-optical switches integrated with a magnet stripe array," Opt. Express **28**(21), 31675–31685 (2020).
16. W. Shi, H. Yun, C. Lin, J. Flueckiger, N. A. F. Jaeger, and L. Chrostowski, "Coupler-apodized Bragg-grating add–drop filter," Opt. Lett. **38**(16), 3068–3070 (2013).
17. D. Mu, H. Qiu, J. Jiang, X. Wang, Z. Fu, Y. Wang, X. Jiang, H. Yu, and J. Yang, "A Four-Channel DWDM Tunable Add/Drop Demultiplexer Based on Silicon Waveguide Bragg Gratings," IEEE Photonics J. **11**(1), 6600708 (2019).
18. A. D. Simard and S. LaRochelle, "Complex apodized Bragg grating filters without circulators in silicon-on-insulator," Opt. Express **23**(13), 16662–16675 (2015).
19. J. Wang and L. R. Chen, "Low crosstalk Bragg grating/Mach-Zehnder interferometer optical add-drop multiplexer in silicon photonics," Opt. Express **23**(20), 26450–26459 (2015).
20. J. Jiang, H. Qiu, G. Wang, Y. Li, T. Dai, D. Mu, H. Yu, J. Yang, and X. Jiang, "Silicon lateral-apodized add–drop filter for on-chip optical interconnection," Appl. Opt. **56**(30), 8425–8429 (2017).
21. D. Liu, M. Zhang, Y. Shi, and D. Dai, "Four-Channel CWDM (de)Multiplexers Using Cascaded Multimode Waveguide Gratings," IEEE Photonics Technol. Lett. **32**(4), 192–195 (2020).
22. D. Liu, H. Wu, and D. Dai, "Silicon Multimode Waveguide Grating Filter at 2 μm," J. Lightwave Technol. **37**(10), 2217–2222 (2019).
23. X. Wang, H. Yu, H. Qiu, Q. Zhang, Z. Fu, P. Xia, B. Chen, X. Guo, Y. Wang, X. Jiang, and J. Yang, "Hitless and gridless reconfigurable optical add drop (de)multiplexer based on looped waveguide sidewall Bragg gratings on silicon," Opt. Express **28**(10), 14461–14475 (2020).
24. N. Saha and A. Kumar, "Toward 100 Micrometer per Refractive Index Unit Sensitive Sensor Using a Compact Long-Period Grating Inscribed Metal Clad Ridge Waveguide," J. Lightwave Technol. **36**(10), 2024–2030 (2018).
25. N. Saha and A. Kumar, "Highly Sensitive Refractive Index Sensor Based on Mode Transition in a Dual Resonance Long Period Grating Inscribed Ridge Waveguide," J. Lightwave Technol. **37**(21), 5576–5582 (2019).
26. M. S. Kwon, "Silicon photonic add-drop filter based on a grating-assisted co-directionally coupled vertical hybrid structure," Opt. Express **27**(8), 11748–11765 (2019).
27. X. Guan, H. Hu, L. K. Oxenløwe, and L. H. Frandsen, "Compact titanium dioxide waveguides with high nonlinearity at telecommunication wavelengths," Opt. Express **26**(2), 1055–1063 (2018).
28. M. Hegeman, F. B. Dijkstra, W. Segerink, S. M. Lee, and Garcia-Blanco, "Development of low-loss TiO2 waveguides," Opt. Express **28**(5), 5982–5990 (2020).
29. S. S. Djordjevic, K. Shang, B. Guan, S. T. S. Cheung, L. Liao, J. Basak, H.-F. Liu, and S. J. B. Yoo, "CMOS-compatible, athermal silicon ring modulators clad with titanium dioxide," Opt. Express **21**(12), 13958–13968 (2013).
30. S. Feng, K. Shang, J. T. Bovington, R. Wu, B. Guan, K.-T. Cheng, J. E. Bowers, and S. J. Ben Yoo, "Athermal silicon ring resonators clad with titanium dioxide for 1.3 μm wavelength operation," Opt. Express **23**(20), 25653–25660 (2015).
31. M. Kulishov, V. Grubsky, J. Schwartz, X. Daxhelet, and D. V. Plant, "Tunable Waveguide Transmission Gratings Based on Active Gain Control," IEEE J. Quantum Electron. **40**(12), 1715–1724 (2004).
32. F. Y.M. Chan and K.S. Chiang, "Analysis of apodized phase-shifted long-period fiber gratings," Opt. Commun. **244**(1-6), 233–243 (2005).

Optics EXPRESS

33. Q. Liu, Z. Gu, J. Sheng Kee, and M. Kyoung Park, "Silicon waveguide filter based on cladding modulated anti-symmetric long-period grating," Opt. Express **22**(24), 29954–29963 (2014).
34. G. Griffel and A. Yariv, "Frequency response and tunability of grating assisted directional couplers," IEEE J.Quantum Electron. **27**(5), 1115–1118 (1991).
35. N. Saha and A. Kumar, "A novel dual resonance long period waveguide grating based highly sensitiverefractive index sensor with reduced temperature sensitivity," Opt. Commun. **474**, 126092 (2020).
36. A. K. Ghatak and K. Thyagarajan, *Introduction to Fiber Optics*. (Cambridge Univ. Press, 1998).
37. Avrutsky, "Integrated Optical Polarizer for Silicon-on-Insulator Waveguides Using Evanescent Wave Coupling to Gap Plasmon–Polaritons," IEEE J. Sel. Top. Quantum Electron. **14**(6), 1509–1514 (2008).
38. A. C. Evans, "Nonlinear optics in titanium dioxide: from bulk to integrated optical devices," Doctoral dissertation. Harvard University (2013).
39. S. M. Tripathi, A. Kumar, R. K. Varshney, Y. B. P. Kumar, E. Marin, and J.-P. Meunier, "Strain and temperature sensing characteristics of single-mode–multimode–single-mode structures," J. Lightwave Technol. **27**(13), 2348–2356 (2009).
40. M. Jacques, A. Samani, E. El-Fiky, D. Patel, Z. Xing, and D. V. Plant, "Optimization of thermo-optic phase-shifter design and mitigation of thermal crosstalk on the SOI platform," Opt. Express **27**(8), 10456–10471 (2019).
41. T. Barwicz and H. A. Haus, "Three-Dimensional Analysis of Scattering Losses Due to Sidewall Roughness in Microphotonic Waveguides," J. Lightwave Technol. **23**(9), 2719–2732 (2005).
42. A. Bera, Y. Marin, M. Harjanne, M. Cherchi, and T. Aalto, "Ultra-low loss waveguide platform in silicon photonics," Proc. SPIE **12006**, 1200603 (2022).
43. Y. Su, Y. Zhang, C. Qiu, X. Guo, and L Sun, "Silicon photonic platform for passive waveguide devices: materials, fabrication, and applications," Adv. Mater. Technol. **5**(8), 1901153 (2020).
44. T. Horikawa, D. Shimura, and T Mogami, "Low-loss silicon wire waveguides for optical integrated circuits.," MRS Commun. **6**(1), 9–15 (2016).
45. M. Musick, J. R. Wendt, P. J. Resnick, M. B. Sinclair, and D. B. Burckela, "Assessing the manufacturing tolerances and uniformity of CMOS compatible metamaterial fabrication," J. Vac. Sci. Technol., B: Nanotechnol. Microelectron.: Mater., Process., Meas., Phenom. **36**(1), 011208 (2018).
46. P. Dong, W. Qian, H. Liang, R. Shafiiha, D. Feng, G. Li, J. E. Cunningham, A. V. Krishnamoorthy, and M. Asghari, "Thermally tunable silicon racetrack resonators with ultralow tuning power," Opt. Express **18**(19), 20298–20304 (2010).
47. F. Duan, K. Chen, and Y. Yu, "Optimization of thermally tunable grating filters with air trench and beam-pillar structures," Opt. Commun. **439**, 239–243 (2019).
48. C. C. Evans, C. Liu, and J. Suntivich, "Low-loss titanium dioxide waveguides and resonators using a dielectric lift-off fabrication process," Opt. Express **23**(9), 11160–11169 (2015).
49. N. S. Droz, K. Preston, J. S. Levy, and M. Lipson, "Device guidelines for WDM interconnects using silicon microring resonators," *Workshop on the Interaction between Nanophotonic Devices and Systems (WINDS)*, **43** 15–18 (2010).
50. D.-X. Xu, J. H. Schmid, G. T. Reed, G. Z. Mashanovich, D. J. Thomson, M. Nedeljkovic, X. Chen, D. V. Thourhout, S. Keyvaninia, and S. K. Selvaraja, "Silicon Photonic Integration Platform—Have We Found the Sweet Spot?" IEEE J. Sel. Top. Quantum Electron. **20**(4), 189–205 (2014).
51. T. Barwicz, M. A. Popovic, M. R. Watts, P. T. Rakich, E. P. Ippen, and H. I. Smith, "Fabrication of add–drop filters based on frequency-matched microring resonators," J. Lightwave Technol. **24**(5), 2207–2218 (2006).
52. D. Conteduca, S.D. Quinn, and T.F. Krauss, "Dielectric metasurface for high-precision detection of large unilamellar vesicles," J. Opt. **23**(11), 114002 (2021).
53. X. Guan, X. Wang, and L. H. Frandsen, "Optical temperature sensor with enhancedsensitivity by employing hybrid waveguides in asilicon Mach-Zehnder interferometer," Opt. Express **24**(15), 16349–16356 (2016).
54. H. St-Yves, P. Bahrami, S. Jean, LaRochelle, and W. Shi, "Widely bandwidth-tunable silicon filter with an unlimited free-spectral range," Opt. Lett. **40**(23), 5471–5474 (2015).
55. M.A. Jithina, K.L. Ganapathi, M. Ambresh, P. Nukala, N.K. Udayashankar, and S. Mohan, "Development of titanium nitride thin film microheaters using laser micromachining," Vacuum **197**, 110795 (2022).